Loading of cobalt on carbon nanofibers

M. Keyser and F.F. Prinsloo

Sasol Technology R&D, KlasieHavenga Road 1, Sasolburg, 1947

Introduction

We are interested in the properties of carbon nanotubes/fibers as support for transition metal catalysts. Carbon nanotubes and nanofibers have similar advantages to activated carbon and carbon black if utilized as support in heterogeneous catalysis (1) but they outperform activated carbon with regard to reproducibility, filterability, stability under oxidising and reducing conditions and abrasiveness (1). It was established that carbon nanofibers interweave during growth, resulting in the formation of mechanically strong tangled agglomerates (1). The agglomerates facilitate an open pore volume, a pore size distribution, a predominant mesoporous structure, high filterability and high mechanical strength, thus rendering carbon nanofibers suitable as support for metal particles in heterogeneous catalysis (1). In addition, the mesoporous structure of carbon nanofibers significantly reduces diffusion transport limitations, which usually occur when activated carbon is utilized as a support.

In this paper, a homogeneous deposition precipitation method employing urea as precipitation method for the preparation of cobalt catalysts was investigated (2). The carbon nanofibers were oxidised in nitric acid before catalyst preparation. A variety of thermal and spectroscopic techniques such as thermogravimetric analysis (TGA), chemisorption, X-ray photoelectron spectroscopy (XPS), transmission electron microscopy (TEM), scanning electron microscopy (SEM), infra-red (FTIR), X-ray diffraction (XRD) and temperature programmed reduction (TPR) were utilized to study the possible influence of the surface oxygen functional groups on the metal dispersion.

Experimental

The synthesis of the carbon nanofibers was performed at atmospheric pressure via the decomposition of acetylene over a stainless steel substrate (SUS310). The stainless steel reactor (volume of the reactor = 340 cm^3) was heated from room temperature to 873 K in 2 hours under a flowing stream of argon (1100 ml min^{-1} STP). Maintaining this temperature**,** the carbon nanofibers were allowed to grow over a period of 30 minutes in a mixture of argon (1100 ml min^{-1} STP) and acetylene (733 ml min^{-1} STP). After cooling in argon**,** the product was stirred overnight at ambient conditions in a mixture of hydrofluoric and hydrochloric acid (HF/HCl = 0.45) to dissolve metals and metal oxides. Afterwards the nanofibers were thoroughly washed with de-ionised water, dried overnight and refluxed in concentrated nitric acid (10 mol dm^{-3}) at 353 K for 4 hours.

For the catalyst preparation, 10 grams of carbon nanofibers were dispersed with 300 cm^3 of de-ionised water for 30 minutes in an ultrasonic bath. This was then slurried with a solution of 250 cm^3 deionized water and 12% m/m cobalt. The slurry was transferred to a 1000 cm^3, 3-neck, indented flask fitted with a top stirrer and pH electrode and an additional 150 cm^3 of deionized water was added to the slurry. The temperature was brought to 363 K after which urea was added with vigorous stirring for 2 hours. The slurry was filtered and washed and then allowed to dry in a vacuum oven at 373 K overnight. The catalysts were heated (20 K min^{-1}) in a nitrogen stream for 1 hour at a desired temperature.

The final samples were analyzed by inductively coupled plasma atomic emission spectrometry (Vista AZ CCD

simultaneous ICP-AES) to determine their elemental composition. The metal contents of the catalysts are given in Table 1. The results to be discussed in this paper are similar for the catalysts with the low and high metal loading and consequently the discussion will focus mainly on the catalysts with the lower metal loading.

Standard equipment such as a JEOL JSM 6000 F scanning electron microscope, Philips EM301 electron microscope operating at 100 kV, Nicolet Magna-IR 550 Spectrometer Series II, Malvern Zetaseizer 2C, Quantum 2000 Scanning SK Microprobe, Perkin Elmer TGA and Micromeritics ASAP 2010 were employed for further characterisation of the carbon nanofibers and cobalt catalysts.

Results and Discussion

Characterization of the carbon nanofibers

TEM and SEM images. A SEM image of the carbon nanofibers shows that the decomposition of acetylene over the stainless steel substrate results in a non-homogeneous mixture of relatively straight and coiled carbon nanofibers which have interwoven during growth and formed agglomerates. The bulk of the sample consists of the coiled carbon nanofibers. The nitrogen adsorption measurements showed that the carbon nanofibers are predominantly mesoporous (BET surface area = 91 m^2 g^{-1} and BJH mesopore surface area = 79 m^2 g^{-1}).

FTIR and XPS analyses. FTIR analysis of the oxidised carbon nanofibers, (Fig. 1) suggests the presence of ketone and carboxyl/lactone acid, phenolic groups and nitro groups on the carbon nanofiber surface. The aromatic stretching coupled to highly conjugated carbonyl groups band is also visible in the FTIR spectrum.

The FTIR measurements showed that calcination at 573 K results in the decomposition of the majority of the surface oxygen functional groups. At this temperature, the phenolic and asymmetric and symmetric NO_2 stretching vibration peaks have disappeared completely. Thus ketone, carboxylic, phenolic and nitro groups decompose if the carbon nanofibers are calcined at 573 K. A peak that remained at ~ 1720 cm^{-1} can be assigned to lactones because these groups decompose between 600 and 950 K (3). Furthermore, if the temperature was increased further to 873 K, the shoulder and peak at ~ 1740 cm^{-1} and ~ 1720 cm^{-1} have disappeared completely.

The XPS wide spectra showed that the total surface oxygen content for the oxidized carbon nanofibers decreases with increasing calcination temperature. The XPS data in the C_{1s} region for the oxidised and calcined carbon nanofibers as well as for a high purity graphite sample is given in Fig. 2. If the asymmetric line profile is removed (Fig. 2) small peaks and shoulders at 285.5, 286.0 (alcohol, ether, phenol), 288.3 (carbonyl, quinone), 288.8 (carboxyl groups) and 289.8 eV (carbonate, CO_2) can be isolated. In correspondence with the FTIR data these peaks become smaller with increasing temperature.

Zeta potential measurements. The dependence of the zeta potentials on pH is shown in Fig. 3. All the zeta potentials were negative and it is only possible to estimate the isoelectronic points (IEP's) for the different samples (4). The estimated isoelectronic point for the unoxidized carbon nanofibers occurred at pH ~ 1.8 while that for the pre-oxidized carbon nanofibers is estimated at pH ~ –3; indicating the introduction of a significant amount of acidic groups during the pre-oxidation step. Anchoring of the cations (e.g. $Co(H_2O)_6^{2+}$) is facilitated via a negatively charged functional group, like for example, a surface carboxyl or carbonyl group. In this respect, it is important to note that the first three pK_a values for the base hydrolysis of $Co(H_2O)_6^{2+}$ in aqueous solutions are 9.7, 9.1 and 12.7 respectively (I = 1 mol dm^{-3}; T = 298 K) (5), and accordingly various soluble cobalt complexes would exist in aqueous solution as function of pH. Besides the existence of these different soluble complexes in aqueous solution, the solid phase $Co(OH)_2$(cr) also exists (5). It only starts to precipitate if the pH is raised to values above pH = 9 (5).

Interaction of precipitated cobalt oxide(s) with the surface of the carbon nanofibers

During the decomposition of the urea at 363 K and the

consequent homogeneous change in the hydroxyl-ion concentration, an electrostatic interaction between the positively charged dissolved cobalt species and the negatively charged surface oxygen functional groups on the carbon fiber support is favoured: Upon adding urea (five times the molar amount of the total cobalt concentration) to a solution of cobalt(II)acetate at a temperature of 363 K under vigorous stirring, visual inspection revealed that, approximately 30 minutes after addition of the urea, the colour of the solution changed to pink with the accompanying precipitation of a pink phase. The onset pH for the formation of the $Co(H_2O)_4(OH)_2$ is ~8.5 (pKa of $Co(H_2O)_5(OH)^+$ = 9.1) and, consequently, under the present experimental conditions, significant amounts of $Co(H_2O)_6^{2+}$ and $Co(H_2O)_5(OH)^+$ will be present in solution during the preparation of the catalysts. During the whole process, the pH of the solution remained at pH ~ 7. Thus $Co(OH)_2$(cr) could not have been precipitated at this pH. It is more likely that the precipitate is the basic cobalt acetate salt, *viz.*, $Co(OAc)_2(1\text{-}x)(OH)_{2x}$ (6). It has been established that this type of compound decomposes to CoO if heat treated in an argon atmosphere at 553 K – 653 K (6d, 6e). Thus in correspondence with the zeta potential results, electrostatic interaction between the negatively charged carbon nanofiber surface and the positively charged cobalt species will be needed for the preparation of the catalysts.

An FTIR spectrum of the carbon nanofibers after catalyst preparation (dried at 393 K) (Fig. 4) showed modification of the infrared absorption carboxylic and phenolic bands. The aromatic stretching band at 1600 cm^{-1} also shifts to lower wave numbers. These observations illustrate an interaction of the metal with the surface carboxylic and phenolic groups. Interaction between the precipitated cobalt with the aromatic ring substituents or conjugated double bonds on the carbon surface is highly likely and this interaction has also been proposed by others (7,8).

Degree of dispersion and surface coverage

Hydrogen chemisorption on cobalt is activated and the extent of activation depends upon the support and metal loading (9,10,11). For this reason, the H_2 chemisorption experiments were performed at an optimum temperature obtained from literature, i.e., 493 K (9). In contrast, the adsorption of CO on cobalt at 298 K is not activated. The adsorption stoichiometry varies from 0.5 to 2.3 molecules of CO per cobalt surface atom depending on the support, metal loading and method of preparation (10). We have found that if the stoichiometry parameter is also changed iteratively during the non-linear regression fit of the CO chemisorption data to the Langmuir equation, a value of $n \approx 1$ resulted.

The crystallite diameters calculated from the H_2 and CO chemisorption data are given in Table 2 together with percentage dispersion, metal surface area, total amount of chemisorbed gas and the H/Co, CO/Co and CO/H ratios. These data shows that the catalysts have small crystallite diameters and high metal dispersion. The CO/H ratios are high indicating incomplete H coverage. Consequently a low hydrogenation activity is expected for the carbon nanofiber supported catalysts. If the metal content increases the, CO/H ratio decreases suggesting that the hydrogenation activity will increase under these conditions (9,10).

Calcination at 573 K results in an increase in the dispersion and the CO/H ratio. Calcination at 873 K results in a further increase in these parameters. As was already shown by the FTIR results, calcination at 573 K results in the decomposition of the majority of the surface oxygen functional groups and after calcination at 873 K, no surface oxygen functional groups could be detected. According to Rodriguez-Reinoso (7), the decomposition of the surface oxygen functional groups increases the strength of the π sites because the electron withdrawing effect exerted by these groups has been neutralized. In line with this reasoning, a worse dispersion is expected when the support's surface is free of surface oxygen functional groups due to repulsive forces between the electropositive cobalt species and the more basic carbon surface. Thus processes other than merely the decomposition of the

surface oxygen functional groups and the resulting influence on the strength of the π sites must be considered in order to explain the observed trends. Calcination at 573 K and 873 K results into the formation of cobalt carbides and cobalt metal indicating that the carbon nanofibers have reducing activity and, at sufficiently high temperatures, the cobalt oxides transfer their oxygen atoms to the support, which is in turn oxidized (12).

TEM images of the carbon nanofiber supported cobalt catalysts are given in Fig. 5. The cobalt crystallites generally appear as dark dots on the surface of the carbon nanofiber support in the TEM images. The individual crystallite diameters were measured with the aid of an image analyzer. The resulting histograms of the crystallite size distributions for the catalysts calcined at 300°C (DPCo4300) and calcined at 600°C (DPCo4600) are given in Fig. 6. The resulting average crystallite diameters turned out to be 7 ± 2 and 25 ± 6 nm for the DPCo4300 and DPCo4600 catalysts respectively. The metal diameters of the two catalysts under consideration differ significantly suggesting that calcination at 873 K as opposed to 573 K does have a large influence on the metal dispersion. The histograms in Fig. 6 also reveal a narrow crystallite distribution for both catalysts, which can be approximated by a normal distribution.

Surface complexes

Difference curves from the TGA data were determined by subtracting the differential curve for the oxidized carbon nanofibers from that for the carbon nanofibers supported cobalt catalysts. The TGA difference curve for the carbon nanofiber supported catalysts (Fig. 7) suggests the formation of CoO at ~ 570 K (6d). The latter is stable in air at ambient temperatures and above 1173 K. As already mentioned, transfer of oxygen atoms by the cobalt oxide species to the support and the consequent oxidation of the support most probably explains the peak at ~ 880 K .

The TPR profiles for the catalysts are given in Fig. 8. The large peak that can be observed above 780 K is due to the catalysed hydrogasification of the carbon nanofibers at these temperatures (12,13,14). For the uncalcined catalyst (DPCo4) and the catalyst calcined at 300°C (DPCo4300), the second peak at ~ 650 K is in correspondence with the one-stage reduction of CoO to Co. The shoulder at ~ 740 K could be due to the decomposition of the more temperature stable surface oxygen functional groups and/or cobalt species that are more difficult to reduce. A TPR profile of the oxidised carbon nanofibers also showed a peak in this region strongly suggesting the former to be the case.

For the DPCo4600 catalyst, it is expected that the heat treatment at 873 K will convert the CoO to Co_3O_4. One is therefore tempted to interpret the two peaks at ~575 K and ~493 K to be due to the reduction of Co_3O_4 (They cannot be due to the decomposition of surface oxygen functional groups due to the calcination at 873 K). However, no Co_3O_4 was detected by XPS or XRD contradicting this possibility. Because the separation between these two peaks is relatively high, it can rather be suggested that they are the consequence of the reduction of cobalt oxides which have different interaction strengths with the support. The larger particles will interact to a lesser extent with the support and would be reduced first. The bulk of the catalyst was reduced at ~ 800 K (peak overlaps with the methane peak). This peak is at a much higher temperature than the peak maximum at ~ 650 K (observed for the other two catalysts) suggesting that calcination at 873 K results in a strong interaction between the carbon nanofiber support and the cobalt with the consequent formation of cobalt species (most probably Co_2C (15)) that are more difficult to reduce than CoO.

XRD analyses (Fig. 9) of the DPCO4300 and DPCO4600 catalysts confirms the formation of cobalt carbides. The peaks at ~30.4^o and ~50.6^o are due to crystalline graphitic carbon and the peaks at ~59.3^o and ~89 ^{o} can be assigned to cobalt carbide (one of the cobalt carbide peaks overlap with the graphitic carbon peak at ~50.6^o). In the case of the DPCo4600 catalyst, cobalt was also detected (peaks at ~52^o, ~60.08^o and ~91^o) which could be due to cobalt particles wrapped in the graphitic carbon support (16). Although not detected by XRD, the presence of amorphous

or microcrystalline CoO phase cannot be totally excluded.

XPS was employed to further investigate the nature of the precipitated cobalt species. The binding energies and peak area ratios are summarized in Table 3. The data confirms the existence of a divalent cobalt oxide species on the carbon nanofiber surface for all the catalysts (the Co_{2p} peak was absent for the DPCo4600 catalyst). Unfortunately the XPS technique does not distinguish between CoO and $Co(OH)_2$ but, as already indicated, literature studies (6d, 6e) showed that the basic acetate salt of cobalt decomposes to CoO at T > 553 K and it is expected that the compound at 781.4 eV is CoO. The shoulder at ~ 786.2 eV is a shake-up peak. No Co_3O_4 could be detected for the catalysts but a large amount of cobalt metal was detected for the DPCo10600 catalyst.

From the wide spectra, the total carbon, oxygen and cobalt content of the catalysts can be calculated (Table 4). Although the total metal content did not change significantly if the catalysts are calcined at 573 K and 873 K respectively, the surface cobalt concentration decreased upon calcination at 873 K to such an extent that it was hardly possible to detect any cobalt species on the surface of the support from the XPS spectra. This suggests that the catalysts calcined at 873 K should have the lowest dispersion. This indicates that the outer atomic layers changed upon heat treatment at 873 K. This could partly be due to the decomposition of the majority of the surface oxygen functional groups but, as already mentioned, other factors should also be considered. It is well-known that thermal desorption of oxygen containing groups increases the number of active sites on a carbon surface (17). Thus, it is possible that the dominant role of the surface functional groups is to provide active sites and thus enhancing the reactivity of the gasification reaction between the carbon material and the oxygen atom (18) from the CoO.

Conclusions

Carbon nanofiber supported cobalt catalysts were prepared according to a deposition precipitation method utilizing urea as precipitating reagent. XPS, FTIR and TGA analyses revealed that oxidation of the carbon nanofibers with nitric acid introduced ketone, carboxylic, phenolic, nitro and lactone groups on the carbon nanofiber surface. During the preparation of the catalysts, an ion exchange reaction between the carboxylic and phenolic groups is favored. The small supported cobalt particles have high dispersions and CO/H ratios and small metal crystallite diameters.

The interaction of the precipitated cobalt oxides with the carbon nanofiber support is influenced to a large extent by the calcination temperature. Calcination of the carbon nanofibers at 573 K resulted in an increase in the interaction between the cobalt particles and the support and an increase in the metal dispersion was established. Under these conditions a small amount of cobalt carbide and cobalt metal was detected by the XRD and XPS analyses. Calcination at 873 K resulted in a further increase in the interaction between the metal and the support leading to increasing amounts of cobalt carbide and cobalt metal. The increase in the interaction between the carbon support and the cobalt species can be explained in terms of the reducing activity of the carbon nanofibers support and, at sufficiently high temperatures, the cobalt oxides transfer their oxygen atoms to the support, which is in turn oxidized. The decomposition of the surface oxygen functional groups results in an increase in the number of active sites on a carbon surface and it is claimed that there dominant role is to provide active sites for the gasification reaction between the carbon material and the oxygen atom from CoO.

The TEM analyses revealed a narrow crystallite distribution with a homogeneous coverage of the support with the metal crystallites.

References

1. a. Geus JW, Van Dillen AJ, Hoogenraad MS. Mater Res Soc Symp Proc. 1995;368:87; b. Hoogenraad MS, Van Leeuwarden RAG, Van Breda Vriesman GJB, Van Dillen AJ, Geus JW. Stud Surf Sci Catal 1995;91:263; c. De Jong KP, Geus JW. Catal Rev-Sci Eng 2000;42(4):481.

2. a. De Jong KP. Current Opinion in Solid State & Materials Science 1999;4:55; b. Doesburg EBM, De Jong KP, Van Hooff JHC. Stud Surf Sci Catal 1999;123:433.

3. Otake Y, Jenkins RG. Carbon 1993;31:109.

4. Bota KB, Abotsi GM, Sims LL. Energy and Fuels 1994;8:937.

5. Plyasunova NV, Zhang Y, Muhammed M. Hydrometall 1998;48:153.

6. a.Doremieux JL. Bull Soc Chim Fr 1967;12:4586; b. Poul L, Jouini N, Fievet F. Chem Mater 2000;12(10):3123; c. Goerge A, Meese-Marktscheffel J, Naumann D, Olbrich A, Schrumpf F. Ger Offen 1996:19 pp; d. Soldatova TA, Tudorovskaya GL, Novozhilova NV, Vashchilo LS, Kuzina ZM. Zh Neorg Khim 1976;21(1):163; e. Mohamed MA, Halawy SA, Ebrahim MMJ. Therm Anal 1994;41(2-3):387.

7. Rodríquez-Reinoso F. Carbon 1998;36:159.

8. Derbyshire FJ, De Beer VHJ, Abotsi GMK, Scaroni AW, Solar JM, Skrovanek DJ. Appl Catal 1986;27:117.

9. Zowtiak JM, Bartholomew CJ. J Catal 1983;83:107.

10. Reuel R, Bartholomew CJ. J. Catal 1984;85:78.

11. Reuel R, Bartholomew C J. Catal 1984;85:78.

12. Gandia lM, Montes M. J Catal 1994;145:276.

13. Guerrero-ruiz A, Sepulveda-Escribano AI. Applied Catal 1984;120:1681.

14. Van Steen E, Prinsloo FF. Submitted for publication in Catalysis Today.

15. Ebbesen TW, Hiura H, Bisher ME, Treacy MJ, Shreeve-Keyer JL, Haushalter RC. Adv Mat 1996;8:155.

16. Saito Y, Yoshikawa T, Okuda M, Fujimoto N, Yamamuro S, Wakoh K, Sumiyama K, Suzuki K, Kasuya A. J Appl Phys 1994;75:134.

17. a Daleya MA, Manguna CL, DeBarrb JA, Rihaa S, Lizziob AA, Donnalsb GL, Economya J. Carbon 1997;35(3):411; b. Mochida I, Kuroda K, Miyamoto S, Sotowa C, Korai Y, Kawano S, Saknishi K, Yasutake A, Yoshikawa M. Energy and Fuels 1997;11:272.

18. *see for example* : a. Mims CA, Pabst JK. Prepr ACS Div Fuel Chem 1980;25:263; b. Chen SG, Yang RT. Energy and Fuels 1997;11:421; c. Moulijn JA, Kapteijn F. NATO ASI Ser, Ser E 1986;105:181; d. Salatino P, Senneca O, Masi S. Carbon 1998;36(4):443.

Acknowledgment

The authors acknowledge Sasol Technology R&D for financial support.

Table 1

Calcination temperature and metal loading of the carbon nanofiber supported cobalt catalysts

Catalyst	Calcination temperature (K)	Cobalt concentration (mass %)
DPCo10	373[a]	10.1
DPCo10300	573; heating rate = 25 K min^{-1}	9.51
DPCo10600	873; heating rate = 25 K min^{-1}	9.81
DPCo4	373	3.80
DPCo4300	573; heating rate = 25 K min^{-1}	3.45
DPCo4600	873; heating rate = 25 K min^{-1}	3.70

Table 2

Comparison of Co_{2p} binding energies for the carbon nanofiber supported cobalt

Catalyst	Binding Energy (eV)	Probable compound	Peak area ratio
DPCo4	782.0	$Co(OAc)_2$ $(1-x)(OH)_{2x}$	1.0
DPCo4300	781.4	CoO	1.0
DPCo4600	No Co_{2p} peak		
DPCo10	782.0	$Co(OAc)_2$ $(1-x)(OH)_{2x}$	1.0
DPCo10300	781.4	CoO	0.83
	778.9	Co metal	0.17
DPCo10600	781.3	CoO	0.64
	778.9	Co metal	0.36

Table 3
Chemisorption results on carbon nanofiber supported cobalt

	Hydrogen chemisorption					CO chemisorption					
Sample	d (nm)	V_m (cm^3g^{-1})	Metal SA (m^2g^{-1})	D (%)	H/Co	d (nm)	V_m (cm^3g^{-1})	Metal SA (m^2g^{-1})	D (%)	CO/Co	CO_{ad}/H_{ad}
DPCo10	9	1.98	7.0	10	0.33	10	9.54	6.5	4	0.33	2.77
DPCo4	8	0.88	3.2	12	0.31	6	2.18	4.0	15	0.33	5.44
DPCo4300	7	0.92	3.4	14	0.36	6	1.96	3.6	18	0.35	4.37
DPCo4600	6	1.16	4.3	17	0.40	5	2.33	4.3	21	0.45	4.71
Co/activated carbon (3 wt % Co)	2	2.91	1.9	29							3.5

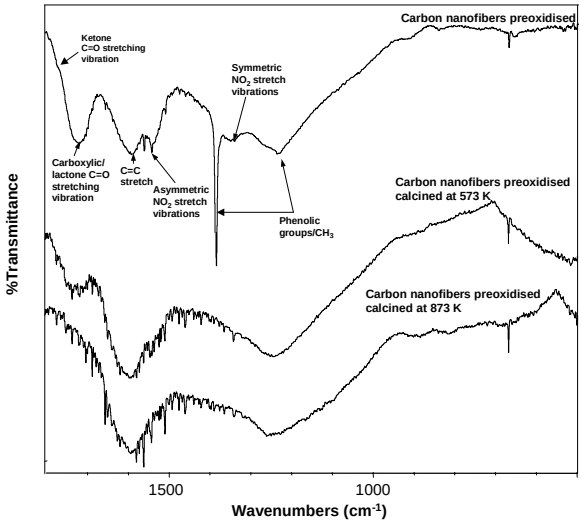

Fig. 1 FTIR spectra of the oxidised and oxidised/calcined carbon nanofibers

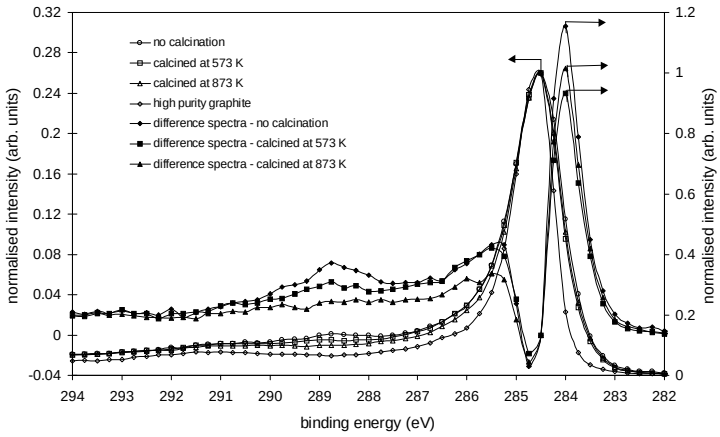

Fig. 2 XPS data in the C1s region for the calcined and uncalcined carbon nanofibers and high purity graphite. The spectra after removal of the asymmetric main contribution are shown on the secondary y-axes.

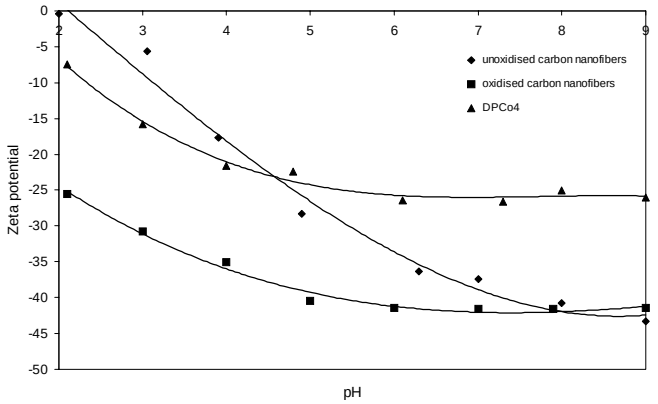

Fig. 3 Variation of Zeta potential of unoxidised and oxidised carbon nanofibers and oxidised carbon nanofibers loaded with cobalt (no calcination).

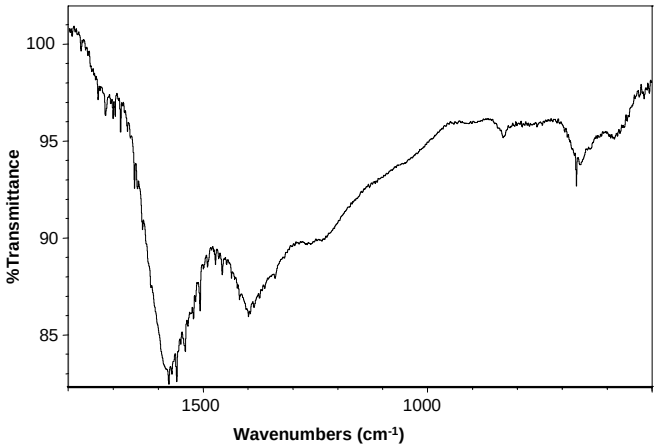

Fig. 4 Infrared spectra of the DPCo4 catalyst (dried at 373 K).

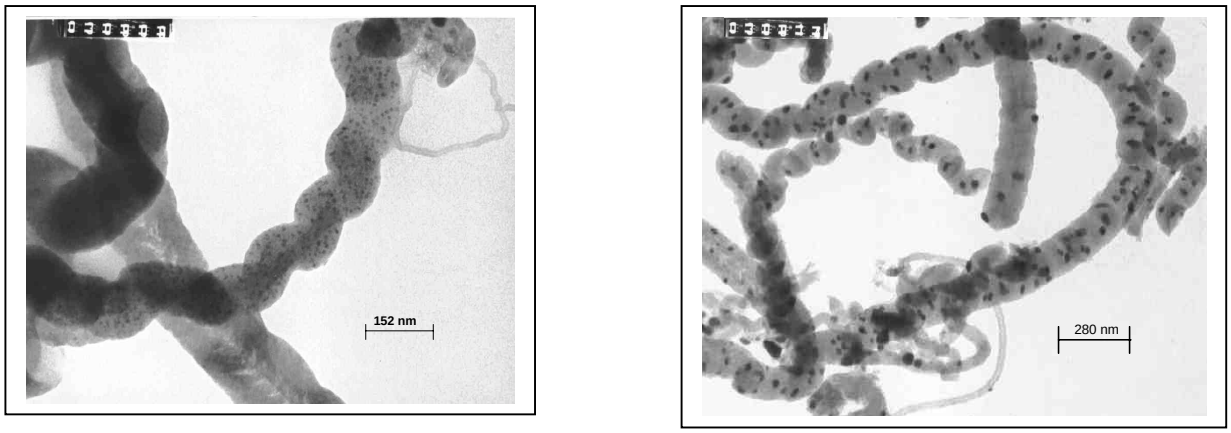

Fig 5 TEM images of the oxidised carbon nanofibers supported cobalt catalysts. a. calcined at 573 K (x130 000). b. Calcined at 873 K (x180 000).

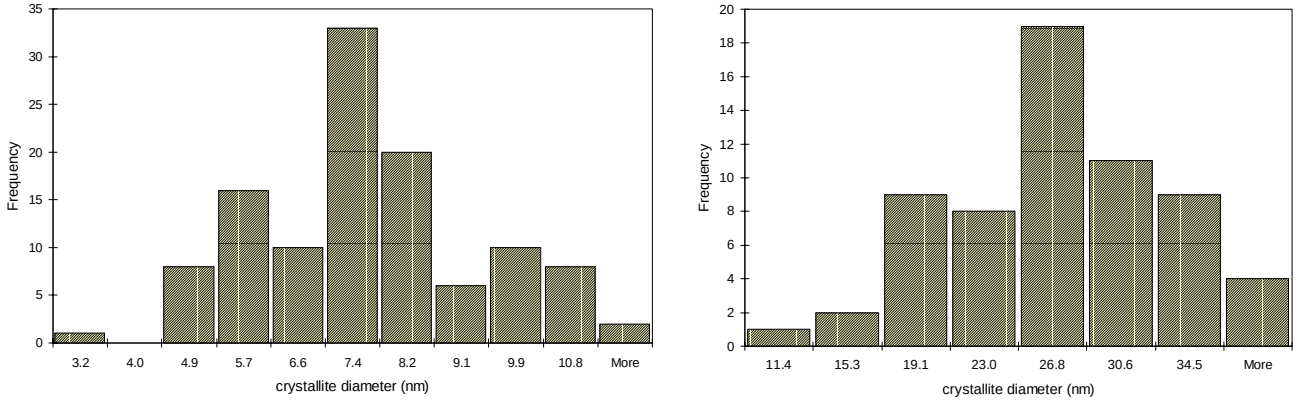

Fig 6 Metal crystallite distribution of the catalysts. a. DPCo4300. b. DPCo600.

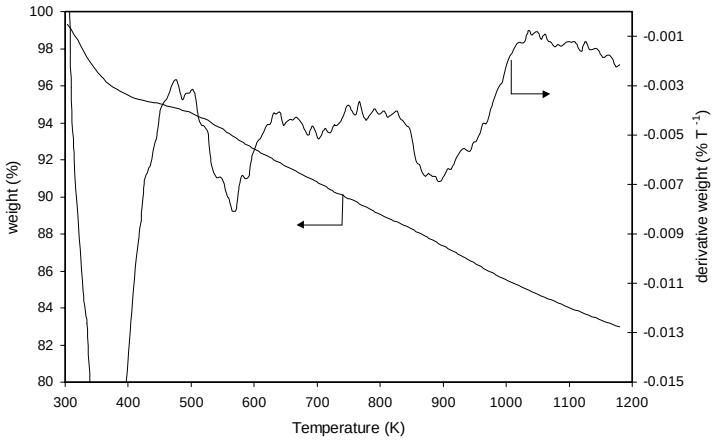

Fig. 7 TGA curve and differential plot of the DPCo4 catalyst (N_2 atmosphere).

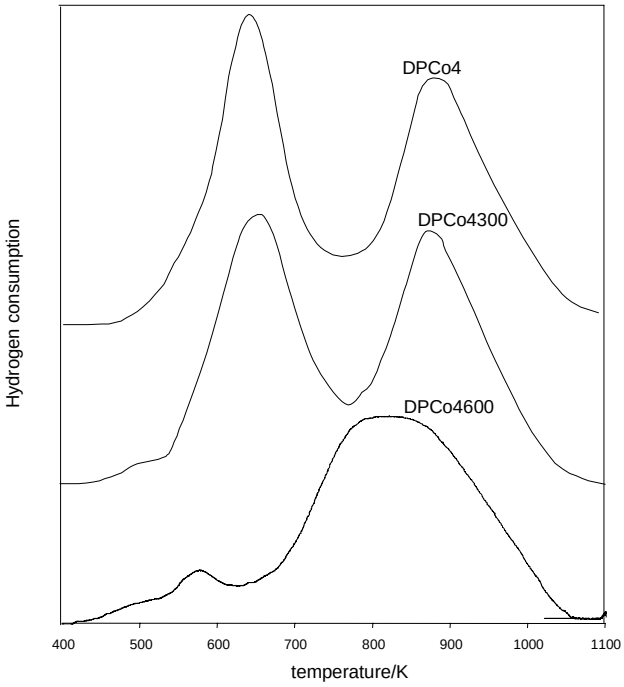

Fig. 8 TPR profiles of the carbon nanofibers supported cobalt oxide catalysts.

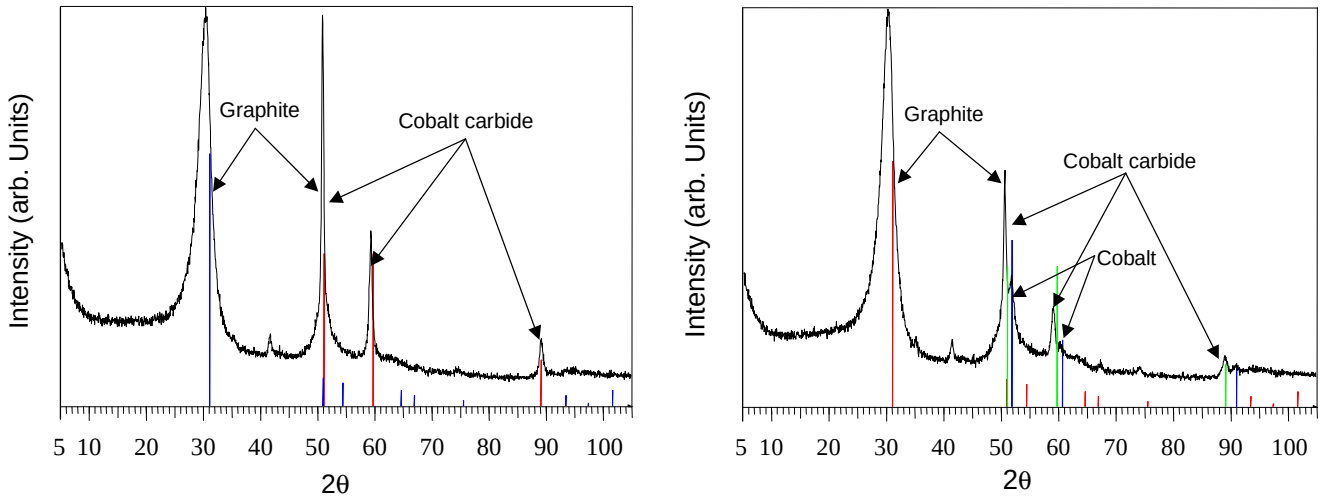

Fig 9 XRD Patterns of the carbon nanofibers supported cobalt oxide catalysts. a. DPCo4300. b. DPCo4600.